G.V.M. Gaias, J.-S. Ardaens, O. Montenbruck
Model of J2 Perturbed Satellite Relative Motion with Time-Varying Differential Drag
Celestial Mechanics and Dynamical Astronomy, Vol. 123, N. 4, 2015, p. 411-433
doi:10.1007/s10569-015-9643-2

Celestial Mechanics

Model of J2 Perturbed Satellite Relative Motion with Time-Varying Differential Drag

--Manuscript Draft--

Manuscript Number:	CELE-D-15-00025R2
Full Title:	Model of J2 Perturbed Satellite Relative Motion with Time-Varying Differential Drag
Article Type:	Original Research
Keywords:	Relative motion; formation flying; relative orbital elements; perturbations
Corresponding Author:	Gabriella Gaias German Space Operations Center Wessling, GERMANY
Corresponding Author Secondary Information:	
Corresponding Author's Institution:	German Space Operations Center
Corresponding Author's Secondary Institution:	
First Author:	Gabriella Gaias
First Author Secondary Information:	
Order of Authors:	Gabriella Gaias
	Jean-Sébastien Ardaens
	Oliver Montenbruck, Dr.
Order of Authors Secondary Information:	
Funding Information:	
Abstract:	This work revisits the modeling of the relative motion between satellites flying in near-circular low-Earth-orbits. The motion is described through relative orbital elements and both Earth's oblateness and differential drag perturbations are addressed. With respect to the former formulation, the description of the J2 effect is improved by including also the changes that this perturbation produces in both relative mean longitude and relative inclination vector during a drifting phase, when a non-vanishing relative semi-major is required. The second major improvement consists in a general empirical formulation to include the mean effects produced by non-conservative perturbations, such as the differential aerodynamic drag acceleration. As a result, in addition to the well-known actions on the relative semi-major axis and on the mean along-track separation, the model is able to reflect the mean variation of the relative eccentricity vector due to atmospheric density oscillations produced by day and night transitions.

Noname manuscript No.
(will be inserted by the editor)

Model of J_2 Perturbed Satellite Relative Motion with Time-Varying Differential Drag

Gabriella Gaias · Jean-Sébastien Ardaens · Oliver Montenbruck

the date of receipt and acceptance should be inserted later

Abstract This work revisits the modeling of the relative motion between satellites flying in near-circular low-Earth-orbits. The motion is described through relative orbital elements and both Earth's oblateness and differential drag perturbations are addressed. With respect to the former formulation, the description of the J_2 effect is improved by including also the changes that this perturbation produces in both relative mean longitude and relative inclination vector during a drifting phase, when a non-vanishing relative semi-major is required. The second major improvement consists in a general empirical formulation to include the mean effects produced by non-conservative perturbations, such as the differential aerodynamic drag acceleration. As a result, in addition to the well-known actions on the relative semi-major axis and on the mean along-track separation, the model is able to reflect the mean variation of the relative eccentricity vector due to atmospheric density oscillations produced by day and night transitions.

Keywords Relative motion · formation flying · relative orbital elements · perturbations

1 Introduction

This work addressees the modeling of the relative motion between two spacecraft flying in near-circular orbits, with the aim to improve the model employed in the following recent formation flying in-flight activities: the Spaceborne Autonomous Formation Flying Experiment (SAFE) (D'Amico et al., 2012), the TanDEM-X Autonomous Formation Flying (TAFF) system (Ardaens et al., 2011a, 2013), and

G. Gaias (✉) · J.-S. Ardaens · O. Montenbruck
GSOC/Space Flight Technology, Münchner Str. 20, 82234 Wessling, Germany
E-mail: gabriella.gaias@dlr.de

J.-S. Ardaens
E-mail: jean-sebastien.ardaens@dlr.de

O. Montenbruck
E-mail: oliver.montenbruck@dlr.de

the Advanced Rendezvous Demonstration using Global Positioning System and Optical Navigation (ARGON) experiment (D'Amico et al., 2013). The post analysis of the flight data collected during ARGON, in fact, presented some minor discrepancies with respect to the expected modeled profiles. In addition, the development of the Autonomous Vision Approach Navigation and Target Identification (AVANTI) experiment (Gaias et al., 2014), scheduled for launch in 2016, required the understanding of the effects determined by the differential aerodynamic drag, due to its major role in this mission scenario. All the aforementioned in-flight activities concern onboard autonomous systems, that have to implement simple and reliable solutions compliant with limited computational resources. Therefore, a simple model able to faithfully represent all the relevant aspects is sought.

The literature presents several relative motion models focused on diverse application scenarios, varying in range of validity, parametrization used, and orbit perturbations included. The effect of the Earth's oblateness J_2 perturbation has been treated in Schweighart and Sedwick (2002) and in Vadali (2009). Schaub and Alfriend (2001) analyzed the J_2 perturbed relative motion through differences of mean orbital elements identifying J_2 invariant relative orbits with respect to the secular effects. Recently Martinusi and Gurfil (2011) and Lara and Gurfil (2012) investigated long-term boundedness conditions for relative orbits under realistic gravitational models. Nevertheless, both the mission typology and the orbit scenarios we are dealing with require frequent maneuver activity. Therefore the effects produced by the Earth's oblateness between two maneuvers can be precisely enough modeled making use of mean orbital elements and first-order truncation in the J_2 parameter.

Studies focused on the effect of the differential aerodynamic drag date back to Leonard et al. (1989), who first introduced the idea of using this acceleration to accomplish formation keeping control. The concept has been further investigated in Bevilacqua and Romano (2008), where the joint effect of J_2 was also accounted for. Both these works make use of the linearized equations of motion in the local Cartesian frame, thus their validity is limited to inter-satellite separations of the order of one kilometer. Moreover, the differential drag is described as a piece-wise constant acceleration in the local along-track direction. More recently Ben-Yaacov and Gurfil (2013) developed a nonlinear method for formation control using differential drag. It is formulated through differences of averaged orbital elements and an exponential model for the atmospheric density is employed. Further research on the utilization of the differential aerodynamic drag as means of formation control aims either at enhancing the performances of the control algorithms (Pérez and Bevilacqua, 2013, 2014) or at improving the capability of modeling the atmospheric density (Pérez et al., 2014).

The AVANTI experiment is intended to demonstrate the capability to perform autonomously rendezvous and receding approaches with respect to a noncooperative client satellite making use of vision-based angles-only measurements. The experiment focuses on mid- to far-range inter-satellite separations, in an environment which is strongly perturbed by the differential aerodynamic drag. The achievable formation control accuracy is driven by the performance of the onboard vision-based navigation system (i.e., at the meter level (Ardaens and Gaias, 2014)). Moreover, the modeling of the differential drag is greatly affected by the uncertainties regarding the knowledge of the attitude-dependent cross-sectional area and drag coefficient of the target, noncooperative, spacecraft. As a result, a

computationally-expensive precise model of the atmosphere density is not really mandatory. In fact, within the AVANTI framework, it is enough to focus on the global effect produced by the differential drag on the relative state using a general and simple empirical formulation, provided that its functional structure is able to reflect one-orbit periodical fluctuations such as those produced by day-night variations of the atmospheric density.

The dynamical model discussed here makes use of the relative orbit elements (ROEs) inherited from the co-location of geostationary satellites (Härting et al., 1988) and afterwards adapted to the formation flying field (D'Amico, 2010). Other similar parametrization forms have been proposed in the literature. Lovell and Tragesser (2004), for example, define relative orbit elements from the geometrical characteristics of the solution of the Hill-Clohessy-Wiltshire equations (HCW) (Clohessy and Wiltshire, 1960). Ichimura and Ichikawa (2008) introduce four constants to parametrize the in-plane components of the solution of the HCW equations. Finally Schaub and Junkins (2003) use differences of absolute non-singular Keplerian orbit elements. Besides the usual characteristics of orbital elements based parametrizations, the ROE formulation here employed, offers a direct geometrical visualization of the effects of the J_2 perturbation on almost-bounded relative orbits (D'Amico and Montenbruck, 2006) and allows easy inclusion of the concept of passive safety of the formation through a certain relative eccentricity/inclination vector separation (Montenbruck et al., 2006). Moreover such ROEs support a straightforward geometrical interpretation of how the geometry of the relative orbits changes under the effect of impulsive maneuvers (Gaias and D'Amico, 2014).

In this frame, the main contributions of this paper are as follows:

- The modeling of the Earth's oblateness effect has been improved by introducing close near-circular orbit assumptions only at the end of the development process. Therefore, in contrast to the previous formulation, the action of the relative semi-major axis on the mean along-track separation and on the y component of the relative inclination vector has been included, which shows the agreement with the collected flight data.
- A framework for transferring the available results in the local Cartesian frame into our ROE-based environment has been defined. It is based on the equivalence that the linearized dynamics expressed either in the local Cartesian frame or through differences of orbital elements share (Sinclair et al., 2014). Afterwards, the linear relations developed in D'Amico (2005) are used for mapping ROEs into the Cartesian frame and vice versa. As a result, the limitations of applicable inter-satellite separation range required in Cartesian formulations are overcome. Moreover, results from both approaches can be merged to increase the understanding of the relative motion problem.
- A general empirical formulation of non-conservative perturbations has been provided, in order to include their mean effects in the ROE time profiles. Its functional structure is derived from the analysis of the dynamical properties of the linearized equations of motion of near-circular orbits performed in Colombo (1989).
- The particular case of the differential aerodynamic drag has been deepened. The analysis shows that whenever the orbit scenario presents day and night transitions, it is not enough to model the differential drag as a piece-wise con-

stant acceleration. In this case, in fact, the oscillating profile of the atmospheric density determines a non-negligible mean linear in time variation of the relative eccentricity vector.

As a result, a simple, though accurate and complete model for the relative motion in near-circular low-Earth-orbits is developed. The relative state expressed by the ROE set is augmented by three constant additional parameters, characterized by a straightforward geometrical interpretation. The first additional parameter is the time derivative of the relative semi-major axis, as already suggested in Gaias et al. (2013). The remaining two are the time derivatives respectively of the x and y components of the relative eccentricity vector, firstly introduced by this work. The so obtained complete state transition matrix can be promptly employed in the relative orbit estimation problem (Ardaens and Gaias, 2014) and in the onboard autonomous maneuver planning problem (Gaias et al., 2013).

After this introduction, the paper continues with the recall of the ROE definition. Section 3 presents the modeling of the Earth's oblateness J_2 perturbation. The transition from the Cartesian to the ROE-based framework is described in Section 4. The modeling of the differential aerodynamic drag is addressed in Section 5. The complete model for the relative motion in low-Earth-orbits is assembled in Section 6. Each modeling-step section is complemented by a numerical validation subsection to support the theoretical results. Finally, the verification through flight data from ARGON is presented in Section 7.

2 Relative motion model

The absolute orbit of a satellite is expressed by the set $\boldsymbol{\alpha} = (a, e, i, \omega, \Omega, u)^{\mathrm{T}}$ of classical Keplerian orbital elements, where $u = M + \omega$ is the spacecraft mean argument of latitude and $n = \sqrt{\frac{\mu}{a^3}}$ is its mean angular motion. The relative motion of a *deputy* spacecraft with respect to one regarded as the *chief* is parametrized using the dimensionless relative orbital elements defined in D'Amico (2010, p. 21), which are the following nonlinear functions of $\boldsymbol{\alpha}$:

$$\delta\boldsymbol{\alpha} = f(\boldsymbol{\alpha}_{\mathrm{d}}, a_{\mathrm{c}}, i_{\mathrm{c}}) - f(\boldsymbol{\alpha}_{\mathrm{c}}, a_{\mathrm{c}}, i_{\mathrm{c}}) = \left(\, \delta a,\, \delta\lambda,\, \delta e_x,\, \delta e_y,\, \delta i_x,\, \delta i_y \,\right)^{\mathrm{T}}, \tag{1}$$

with:

$$f(\boldsymbol{\alpha}, a_{\mathrm{c}}, i_{\mathrm{c}}) = \begin{pmatrix} a/a_{\mathrm{c}} \\ u + \Omega\cos i_{\mathrm{c}} \\ e\cos\omega \\ e\sin\omega \\ i \\ \Omega\sin i_{\mathrm{c}} \end{pmatrix}, \tag{2}$$

where the subscripts "c" and "d" respectively label the *chief* and *deputy* satellites.[1] The first two components of the relative state $\delta\boldsymbol{\alpha}$ are the relative semi-major axis δa and the relative mean longitude $\delta\lambda$. The remaining components constitute the

[1] The relationship between ROEs and the relative Cartesian state is discussed later in Section 4.

relative eccentricity vector $\delta\mathbf{e}$ and the relative inclination vector $\delta\mathbf{i}$ whose Cartesian and polar notations are here recalled:

$$\delta\mathbf{e} = \begin{pmatrix} \delta e_x \\ \delta e_y \end{pmatrix} = \delta e \begin{pmatrix} \cos\varphi \\ \sin\varphi \end{pmatrix} \qquad \delta\mathbf{i} = \begin{pmatrix} \delta i_x \\ \delta i_y \end{pmatrix} = \delta i \begin{pmatrix} \cos\theta \\ \sin\theta \end{pmatrix}, \tag{3}$$

with φ denoting the perigee and θ the ascending node of the relative orbit (see Figure 1).

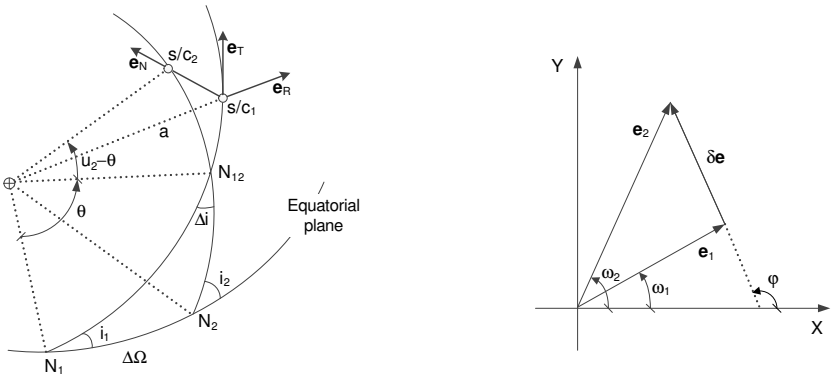

Fig. 1 Definition of ascending node θ (left) and perigee φ (right) of the relative orbit (D'Amico and Montenbruck, 2006).

Recalling the parametrizations mentioned in the introduction, Lovell and Tragesser (2004) relative orbit elements set $(a_e, x_d, y_d, \beta, z_{\max}, \psi)$ corresponds to $(2a\delta e, a\delta a, a\delta\lambda, \varphi, a\delta i, \theta)$; whereas Ichimura and Ichikawa (2008) four in-plane constants (a, d, c, α) correspond to $(a\delta e, a\delta\lambda, a\delta a/2, \varphi)$. Finally, if the chief satellite flies on a circular orbit, the orbit element difference set $\mathbf{e}_\mathrm{d} - \mathbf{e}_\mathrm{c}$ of Schaub and Junkins (2003) becomes $(a\delta a, \delta u, \delta i_x, \delta e_x, \delta e_y, \delta i_y / \sin i_\mathrm{c})$, where the relative mean latitude δu is related to the relative mean longitude by:

$$\delta u = \delta\lambda - \delta i_y \cot i_\mathrm{c}. \tag{4}$$

This work focuses on the relative motion between satellites flying in near-circular orbits. In this frame, the linearized unperturbed dynamics is described by the HCW equations and the ROEs of Equation (1) are their integration constants (D'Amico, 2005).

3 Model of the Earth bulge perturbation

The non-homogeneous mass distribution of the Earth generates a gravity field that can be modeled through a potential function comprising zonal, tesseral, and sectorial terms. With respect to the uniform mass distribution, the main perturbation effect is produced by the second order zonal contribution J_2, which induces the

following secular variations of the absolute Keplerian elements (Brower, 1959):

$$\begin{cases} \dfrac{da}{dt} = \dfrac{de}{dt} = \dfrac{di}{dt} = 0 \\ \dfrac{d\Omega}{dt} = -3\gamma n \cos i \\ \dfrac{d\omega}{dt} = \dfrac{3}{2}\gamma n(5\cos^2 i - 1) \\ \dfrac{dM}{dt} = \dfrac{3}{2}\gamma\eta n(3\cos^2 i - 1) \end{cases}, \tag{5}$$

where $\eta = \sqrt{1-e^2}$, $\gamma = \dfrac{J_2}{2}\dfrac{R_\oplus^2}{a^2\eta^4}$, and $R_\oplus$ is the Earth radius.

Regarding the relative motion, the secular variations of the ROEs can be obtained from the differentiation of the secular variations of the Keplerian elements of each satellite making use of the ROEs definition of Equation (1). Subsequently, these nonlinear expressions can be linearized in the vicinity of the chief orbit by keeping the first order term in the absolute elements difference $\Delta\alpha_j$:

$$\frac{d}{dt}(\delta\alpha_i) = \frac{d}{dt}\left(f_i(\boldsymbol{\alpha})_\mathrm{d} - f_i(\boldsymbol{\alpha})_\mathrm{c}\right) \approx \sum_j \left.\frac{\partial g_i}{\partial \alpha_j}\right|_\mathrm{c} \Delta\alpha_j, \tag{6}$$

where $g_i = df_i/dt$.

In the following steps all the expressions of Equation (6) are derived. Contrary to D'Amico (2010), the simplifications due to close near-circular orbits are only introduced at the end of the process, in order to assess which contributions have to be retained to achieve a simple model though able to represent all the meaningful aspects.

According to Equations (1) and (5), $\delta\dot{a} = \delta\dot{i}_x = 0$.

The time derivative of the x component of the eccentricity vector is given by:

$$\frac{d}{dt}(e_x) = g_3 = -\frac{3}{2}\gamma ne\sin\omega(5\cos^2 i - 1), \tag{7}$$

and its partials with respect to the absolute elements are:

$$\begin{aligned} \frac{\partial g_3}{\partial a} &= \frac{21}{4}\gamma n(5\cos^2 i - 1)e_y\frac{1}{a}, \\ \frac{\partial g_3}{\partial e} &= -3\gamma n(5\cos^2 i - 1)\sin\omega\left(\frac{1}{2} + 2\left(\frac{e}{\eta}\right)^2\right), \\ \frac{\partial g_3}{\partial \omega} &= -\frac{3}{2}\gamma n(5\cos^2 i - 1)e_x, \\ \frac{\partial g_3}{\partial i} &= \frac{15}{2}\gamma n e_y \sin(2i). \end{aligned} \tag{8}$$

The time derivative of the y component of the eccentricity vector is given by:

$$\frac{d}{dt}(e_y) = g_4 = \frac{3}{2}\gamma ne\cos\omega(5\cos^2 i - 1), \tag{9}$$

and its partials with respect to the absolute elements are:

$$\begin{aligned}
\frac{\partial g_4}{\partial a} &= -\frac{21}{4}\gamma n(5\cos^2 i - 1)e_x\frac{1}{a},\\
\frac{\partial g_4}{\partial e} &= 3\gamma n(5\cos^2 i - 1)\cos\omega\left(\frac{1}{2} + 2\left(\frac{e}{\eta}\right)^2\right),\\
\frac{\partial g_4}{\partial \omega} &= -\frac{3}{2}\gamma n(5\cos^2 i - 1)e_y,\\
\frac{\partial g_4}{\partial i} &= -\frac{15}{2}\gamma n e_x \sin(2i).
\end{aligned} \tag{10}$$

The linearized expressions for the time derivative of the relative eccentricity vector are obtained making use of $\delta e_x \approx \cos\omega\Delta e - e\sin\omega\Delta\omega$ and $\delta e_y \approx \sin\omega\Delta e + e\cos\omega\Delta\omega$, (valid for Δe and $\Delta\omega$ small which is fully acceptable for formations with no assumptions on δa, $\delta\lambda$, and e_c):

$$\begin{aligned}
\delta\dot{e}_x &= +\frac{21}{4}\gamma n(5\cos^2 i - 1)e_y\delta a - \frac{3}{2}\gamma n(5\cos^2 i - 1)\delta e_y + \frac{15}{2}\gamma n\sin(2i)e_y\delta i_x,\\
\delta\dot{e}_y &= -\frac{21}{4}\gamma n(5\cos^2 i - 1)e_x\delta a + \frac{3}{2}\gamma n(5\cos^2 i - 1)\delta e_x - \frac{15}{2}\gamma n\sin(2i)e_x\delta i_x.
\end{aligned} \tag{11}$$

According to Equation (11) the contributions proportional to δa and δi_x are smaller than the remaining ones by a factor e. Therefore when dealing with near-circular orbits, Equation (11) can be simplified to:

$$\begin{aligned}
\delta\dot{e}_x &= -\varphi' n\delta e_y,\\
\delta\dot{e}_y &= +\varphi' n\delta e_x,
\end{aligned} \tag{12}$$

in agreement with D'Amico (2010), where the expression $\varphi' = d\varphi/du = \frac{3}{2}\gamma(5\cos^2 i - 1)$ was introduced in order to integrate Equation (12) in a closed form.

The time derivative of the y component of the relative inclination vector is computed from

$$g_6 = -3\gamma n\cos i\sin i_c \qquad \text{and} \qquad \frac{d}{dt}(\delta i_y) = \sum_j \left.\frac{\partial g_6}{\partial \alpha_j}\right|_c \Delta\alpha_j. \tag{13}$$

Since the partials are evaluated at the chief's orbit, the subscript "c" is now dropped:

$$\begin{aligned}
\frac{\partial g_6}{\partial a} &= \frac{21}{2}\gamma n\cos(i)\sin(i)\frac{1}{a},\\
\frac{\partial g_6}{\partial e} &= -12\gamma n\cos(i)\sin(i)\frac{e}{\eta^2},\\
\frac{\partial g_6}{\partial i} &= 3\gamma n\sin^2 i,
\end{aligned} \tag{14}$$

leading to:

$$\delta\dot{i}_y = \frac{21}{4}\gamma n\sin(2i)\delta a + 3\gamma n\sin^2 i\delta i_x. \tag{15}$$

As accomplished for Equation (11), here only the contributions proportional to δa and δi_x can be retained, since for near-circular orbits $\eta \approx 1$ and the term in Δe is of order e smaller than the other two.

Finally, by making use of Equation (4), the time derivative of the mean argument of latitude is firstly computed according to:

$$\frac{d}{dt}(u) = g_2 - \frac{d\Omega}{dt}\cos i_c = \tilde{g}_2 = \frac{3}{2}\gamma n\left(K + \eta H\right), \tag{16}$$

with $K = 5\cos^2 i - 1$ and $H = 3\cos^2 i - 1$. The partials of $\tilde{g}_2$ with respect to the absolute elements are:

$$\begin{aligned}
\frac{\partial \tilde{g}_2}{\partial a} &= -\frac{21}{4}\gamma n\left(K + \eta H\right)\frac{1}{a}, \\
\frac{\partial \tilde{g}_2}{\partial e} &= 3\gamma n e\left(2\frac{K}{\eta^2} + \frac{3}{2}\frac{H}{\eta}\right), \\
\frac{\partial \tilde{g}_2}{\partial i} &= -\frac{3}{2}\gamma n \sin(2i)\left(3\eta + 5\right),
\end{aligned} \tag{17}$$

leading to the following expression for the time derivative of the relative mean argument of latitude:

$$\delta\dot{u} = -\frac{21}{4}\gamma n\left(K + \eta H\right)\delta a + 3\gamma n\left(2\frac{K}{\eta^2} + \frac{3}{2}\frac{H}{\eta}\right)\left(e_x\delta e_x + e_y\delta e_y\right) - \frac{3}{2}\gamma n\sin(2i)\left(3\eta + 5\right)\delta i_x. \tag{18}$$

By neglecting again the contributions smaller of order e, one obtains:

$$\delta\dot{u} = -\frac{21}{4}\gamma n\left(K + \eta H\right)\delta a - \frac{3}{2}\gamma n\sin(2i)\left(3\eta + 5\right)\delta i_x. \tag{19}$$

Equations (15) and (19) present additional terms (i.e., proportional to δa) with respect to the Equation (2.28) developed in (D'Amico, 2010). On the other hand, the coefficients multiplying δi_x converge to the previous results, when $\eta = 1$.

To conclude this section, the expressions of Equations (12)-(15)-(19) can be integrated with respect to the time. The relative mean argument of latitude over time is given by:

$$\delta u(t) = ndt\left(-\frac{3}{2} - \frac{21}{4}\gamma(K + \eta H)\right)\delta a_0 + ndt\left(-\frac{3}{2}\gamma\sin(2i)(3\eta + 5)\right)\delta i_{x0} + \delta u_0, \tag{20}$$

where $dt = t - t_0$, "0" labels all the initial ROE quantities, and the term $-\frac{3}{2}ndt\delta a_0$ represents the solution of the Keplerian relative motion.

The relative mean longitude over time is obtained from Equation (4) and the state transition matrix for the relative motion subject to the J_2 perturbation is given by:

$$\delta\boldsymbol{\alpha}(t) = \boldsymbol{\Phi}(t, t_0)\delta\boldsymbol{\alpha}_0 = \left(\boldsymbol{\Phi}_{\mathrm{HCW}}(t, t_0) + \boldsymbol{\Phi}_{\mathrm{J_2}}(t, t_0)\right)\delta\boldsymbol{\alpha}_0, \tag{21}$$

with:

$$\boldsymbol{\Phi}_{\mathrm{HCW}}(t, t_0) = \begin{bmatrix} 1 & 0 & 0 & 0 & 0 & 0 \\ -\frac{3}{2}ndt & 1 & 0 & 0 & 0 & 0 \\ 0 & 0 & 1 & 0 & 0 & 0 \\ 0 & 0 & 0 & 1 & 0 & 0 \\ 0 & 0 & 0 & 0 & 1 & 0 \\ 0 & 0 & 0 & 0 & 0 & 1 \end{bmatrix}, \tag{22}$$

and

$$\boldsymbol{\Phi}_{J_2}(t,t_0) = ndt \begin{bmatrix} 0 & 0 & 0 & 0 & 0 & 0 \\ -\frac{21}{4}\gamma H(\eta+1) & 0 & 0 & 0 & -\frac{3}{2}\gamma\sin(2i)(3\eta+4) & 0 \\ 0 & 0 & 0 & -\varphi' & 0 & 0 \\ 0 & 0 & +\varphi' & 0 & 0 & 0 \\ 0 & 0 & 0 & 0 & 0 & 0 \\ \frac{21}{4}\gamma\sin(2i) & 0 & 0 & 0 & +3\gamma\sin^2 i & 0 \end{bmatrix}. \tag{23}$$

The relative motion model of Equations (21)-(23) results fully linear in the initial relative state $\delta\boldsymbol{\alpha}_0$.

3.1 Numerical validation

This section focuses on the numerical validation of the improvement in the modeling of the J_2 discussed above, whereas the assessment of the overall model accuracy is performed later in section 6.1, evaluating the complete model of the relative motion.

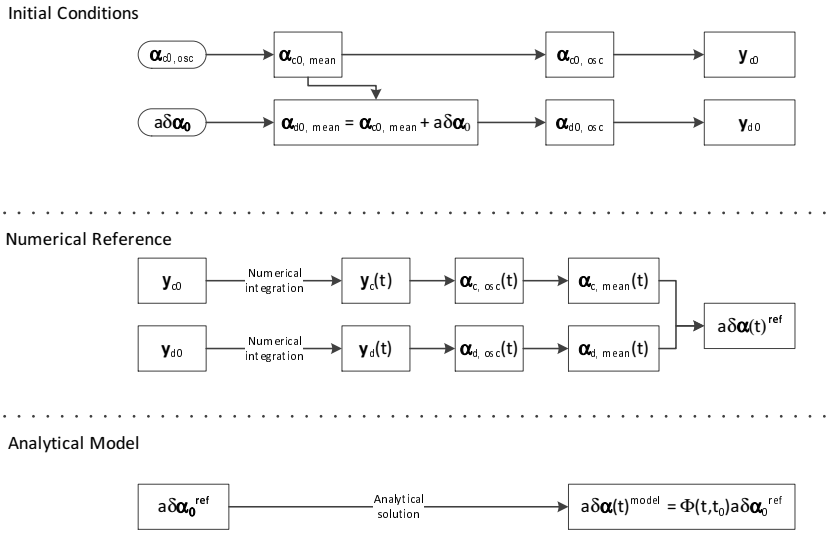

Fig. 2 Setup for the numerical validation of the J_2 perturbation modeling.

The simulation setup employed to validate the model discussed so far is depicted in Figure 2. The initial conditions are defined through the osculating Keplerian elements of the chief satellite $\boldsymbol{\alpha}_{\mathrm{c0,\ osc}}$ at time t_0 and the initial dimensional mean relative state $a\delta\boldsymbol{\alpha}_0$, where a is the mean semi-major axis of the chief. These inputs are used to compute the corresponding satellite's initial states (i.e., $\mathbf{y}_{\mathrm{c0}}$ and $\mathbf{y}_{\mathrm{d0}}$) in the inertial J2000 reference frame, by following a chain of transformations comprising the nonlinear relations between Cartesian state and orbital elements and the transformations from osculating to mean elements defined in Schaub and

Table 1 Absolute and relative orbits initial conditions for the simulations across the paper.

Chief orbit						
	SSO	$h = 500$ (km)	$e = 0.001$	$\Omega_0 = f(t_0, \text{LTAN})$	$\omega_0 = 0$	$M_0 = 0$
Relative Orbits (RO)						
	$a\delta a_0$	$a\delta\lambda_0$	$a\delta e_{x0}$	$a\delta e_{y0}$	$a\delta i_{x0}$	$a\delta i_{y0}$
	(m)	(m)	(m)	(m)	(m)	(m)
RO1	0	5000	30	250	-10	300
RO2	-200	5000	30	250	-10	300

Junkins (2003, p. 693-696). Mean absolute elements are used in order to remove short and long period oscillations generated by the non-homogeneous Earth mass distribution.

The *reference* orbits are obtained via numerical integration (i.e., using the 5^{th} order DOPRI5 integrator of Dormand and Prince (1980) at 10 s step size) from the initial state. During this preliminary validation phase, both satellites are simply considered to move under the combined acceleration of a point mass and the J_2 term of the gravitational potential. The dimensional reference ROEs (i.e., $a\delta\boldsymbol{\alpha}^{\text{ref}}$) are computed step by step from the mean orbital elements of the two satellites.

Finally the modeled ROEs (i.e., $a\delta\boldsymbol{\alpha}^{\text{model}}$) are analytically derived making use of the state transition matrix of Equations (21)-(23), starting from the initial reference relative state $a\delta\boldsymbol{\alpha}_0^{\text{ref}}$, to avoid the numerical errors introduced by the initialization process from the input $a\delta\boldsymbol{\alpha}_0$.

Table 1 summarizes the initial conditions for the simulations presented across the paper. The chief satellite flies on a Sun-synchronous orbit (SSO) of eccentricity 0.001, 500 km high. Initial time and local time of the ascending node (LTAN) vary depending on the considered scenario, whereas at the initial time the spacecraft is in $\omega_0 = M_0 = 0$. Two relative orbits are considered (i.e., labeled with RO1 and RO2) described by two sets of ROEs. Both relative orbits present a mean along-track separation of 5 km and an almost parallel relative eccentricity/inclination vector configuration. RO1 is a non-drifting orbit (i.e., $\delta a = 0$), whereas RO2 drifts apart from the chief satellite (i.e., $a\delta a = -200$ m).

Since the changes in the model affect only the relative mean longitude and the y component of the relative inclination vector, only $a\delta\lambda$ and $a\delta i_y$ will be discussed. Figures 3 and 4 show the errors over time, which are defined as the difference between $a\delta\boldsymbol{\alpha}^{\text{model}}$ and $a\delta\boldsymbol{\alpha}^{\text{ref}}$ for the two considered components. In these plots the black dots mark the model of Equations (21)-(23), whereas the gray ones denote the model previously employed in our works (Ardaens and D'Amico, 2009; D'Amico et al., 2012, 2013).

Both simulations span 15 orbits, which corresponds to approximately one day.

Numerical results show that in the case of non-drifting relative motion the two models are the same, being $\eta \approx 1$, with the eccentricity of Table 1. When a certain drift occurs, instead, the model of Equations (21)-(23) is more accurate, since it accounts for the effects driven by the presence of a non-vanishing relative semi-major axis δa. These corrections in the model remove the numerical discrepancies detected in some phases of the ARGON experiment (see Section 7), where a

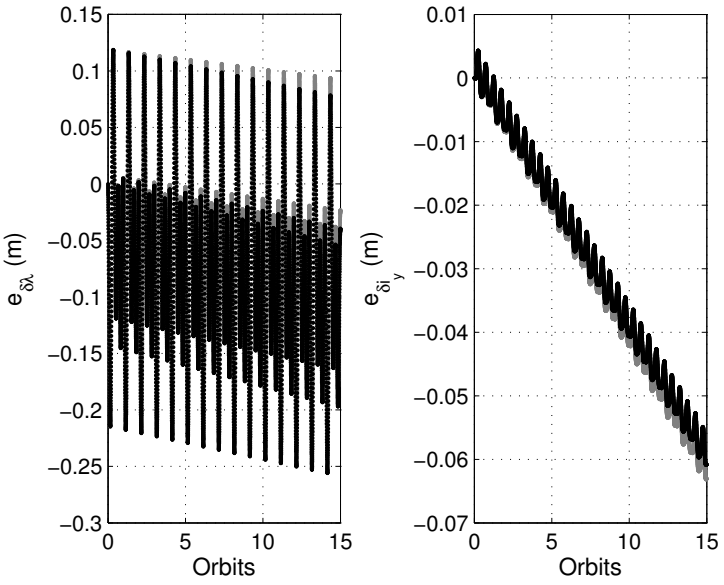

Fig. 3 Modeling error for RO1 of Table 1: improved model (black), former model (gray).

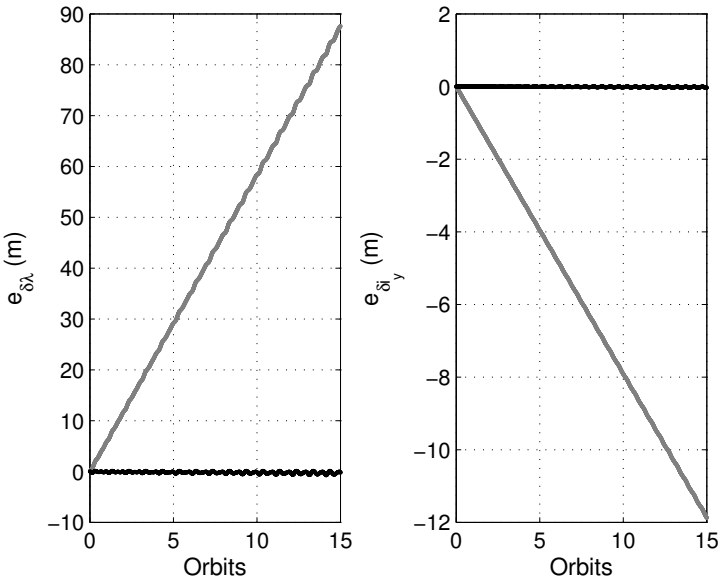

Fig. 4 Modeling error for RO2 of Table 1: improved model (black), former model (gray).

rendezvous was taking place, and the J_2 perturbation was the predominant active perturbation.

4 From Cartesian to ROEs-based models

The current literature offers several solutions for tackling the relative motion problem in the local Cartesian frame centered on one of the two satellites. This section focuses on how to integrate such results into the ROE-based model.

The proposed approach makes use of the results of Sinclair et al. (2014), which show that the linearized relative dynamics described either in the local Cartesian frame or through orbital elements differences share an equivalence through a linearized transformation. In this frame, Sinclair et al. (2014) propose a method to *calibrate* the initial conditions for the linearized Cartesian equations of motion, to reduce the linearization error that occurs when employing initial conditions purely calculated from kinematics. Such calibration consists in mapping linearly the orbital elements differences into the Cartesian relative state $\mathbf{x}$ through the matrix developed by Schaub and Junkins (2003, p. 596-601).

Within the ROEs frame, and when the satellite orbits are near-circular, the linear relations that map ROEs to the Cartesian relative state are developed in D'Amico (2005), and here recalled for completeness:

$$\mathbf{x} = \mathbf{M} a\delta\boldsymbol{\alpha},$$
$$\mathbf{M}(u,n) = \begin{bmatrix} 1 & 0 & -\cos u & -\sin u & 0 & 0 \\ 0 & 1 & 2\sin u & -2\cos u & 0 & 0 \\ 0 & 0 & n\sin u & -n\cos u & 0 & 0 \\ -\frac{3}{2}n & 0 & 2n\cos u & 2n\sin u & 0 & 0 \\ 0 & 0 & 0 & 0 & \sin u & -\cos u \\ 0 & 0 & 0 & 0 & n\cos u & n\sin u \end{bmatrix}. \tag{24}$$

Here $\mathbf{x} = (x, y, dx/dt, dy/dt, z, dz/dt)^{\mathrm{T}}$ with x, y, z respectively labeling the radial, along-track and normal directions of the local orbital frame. Both $\mathbf{M}$ and its inverse show that the in-plane components are decoupled from the out-of-plane ones.

Therefore the integration of Cartesian coordinates-based results into the ROEs frame can be accomplished following the chain of transformations depicted in Figure 5.

According to it, ROEs initial conditions $a\delta\boldsymbol{\alpha}_0$ generate an approximated Cartesian initial state $\mathbf{x}_0^{\mathrm{approx}}$, which slightly differs from the true relative state $\mathbf{x}_0^{\mathrm{ref}}$ obtained from the inertial states of the two satellites. The relative state evolution from $\mathbf{x}_0^{\mathrm{approx}}$ models better the true state $\mathbf{x}(t)^{\mathrm{ref}}$, due to a lower degree of nonlinearity for the orbital element differences compared with the Cartesian coordinates (Sinclair et al., 2014). As an example, the case of RO1 of Table 1 is reported in Figure 6, where HCW equations are used and no perturbations are included. The plots present the time evolution of the modeling errors for the 4 in-plane components of the relative state (i.e., radial and along-track positions and velocities). The error is computed as the difference between $\mathbf{x}(t)^{\mathrm{model}}$ and $\mathbf{x}(t)^{\mathrm{ref}}$; whereas the modeled states evolve from $\mathbf{x}_0^{\mathrm{approx}}$ (i.e., black error) and from $\mathbf{x}_0^{\mathrm{ref}}$ (i.e., gray error). This example shows that at 5 km of mean along-track separation, the linearized Cartesian model would not be employable without the calibration of the initial conditions, which is obtained through an orbital elements formulation.

As depicted in the bottom part of Figure 5, whenever a closed form solution is available in the Cartesian frame, this can be mapped into ROEs using the inverse of $\mathbf{M}$ at the proper time (i.e., u). As a result, the $a\delta\boldsymbol{\alpha}(t)^{\mathrm{model}}$ framed by the gray box

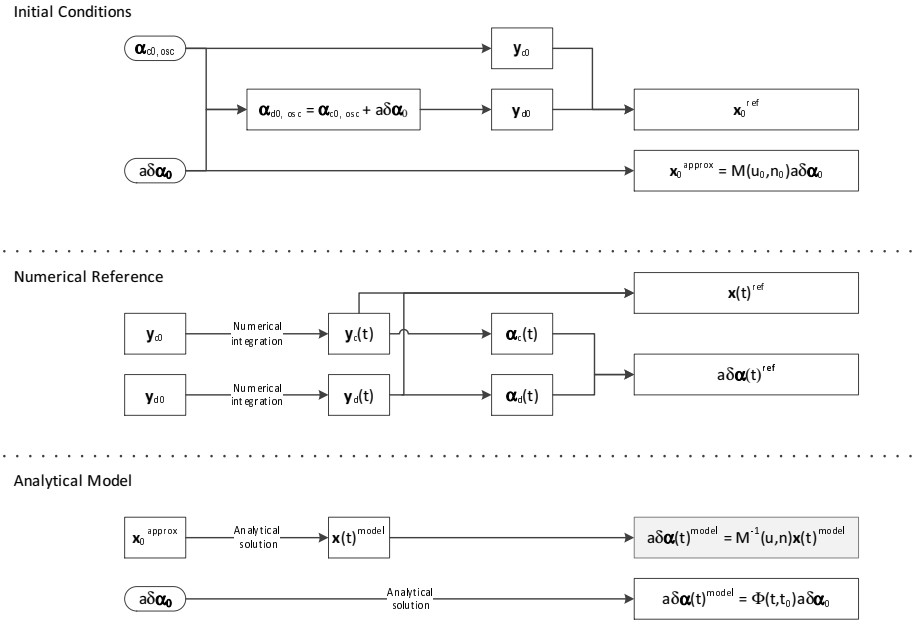

Fig. 5 Equivalence of the linearized relative motion in Cartesian and ROEs parametrization.

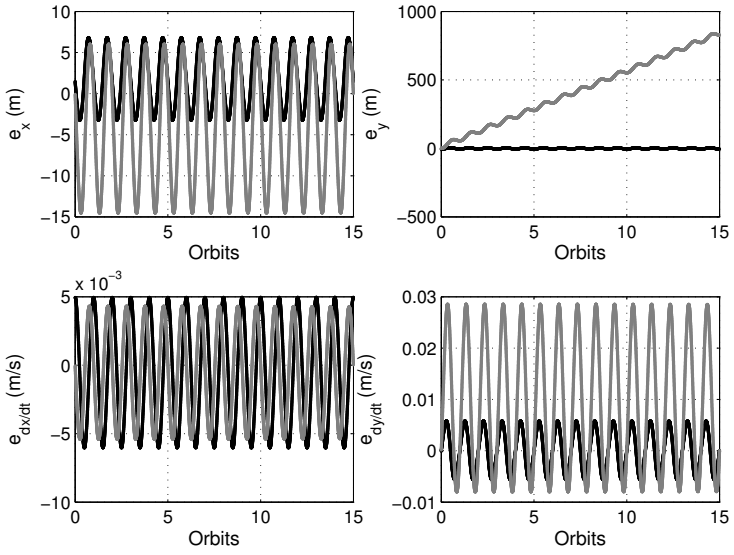

Fig. 6 Error committed by the HCW dynamical model employing $\mathbf{x}_0^{\text{approx}}$ (black) or $\mathbf{x}_0^{\text{ref}}$ (gray) as initial conditions, for a mean along-track separations of circa 5000 m.

is achieved. Nevertheless, since $\mathbf{x}(t)^{\text{model}}$ has a closed form expression, the complete chain can be also written in the form of a state transition matrix that evolves the initial state $a\delta\boldsymbol{\alpha}_0$ into $a\delta\boldsymbol{\alpha}(t)^{\text{model}}$. Therefore, the proposed methodology merges the advantages of a ROE-based approach (e.g., usable at rather large inter-satellite separations, direct geometrical interpretation of the relative orbit) with the rich available literature of Cartesian models for the relative motion.

The numerical validation of the approach is accomplished by comparing the modeled ROEs with the reference $a\delta\boldsymbol{\alpha}(t)^{\text{ref}}$ directly computed from the absolute elements of the two satellites obtained from the true inertial states in J2000 (see Section 5.3). In all these transformations orbital elements are the osculating ones.

5 Modeling the effect of the differential aerodynamic drag

The upper layers of the Earth atmosphere that impact a satellite produce a perturbation acceleration modeled as:

$$\mathbf{d}_{\text{drag}}^{\text{J2000}} = -\frac{1}{2}\rho \left\|\mathbf{v} - \mathbf{v}_{\text{atm}}\right\| (\mathbf{v} - \mathbf{v}_{\text{atm}}) \frac{SC_D}{m}, \tag{25}$$

with ρ denoting the atmospheric density, S the impact cross-sectional area, C_D the drag coefficient, and m the mass of the spacecraft. The quantity $\frac{SC_D}{m}$ is called ballistic coefficient C_B.

At a relative level, for inter-satellite separations of circa 10 km, the following simplified model can be employed:

$$\mathbf{d}_{\text{d-drag}}^{\text{RTN}} = \begin{pmatrix} 0 \\ -\frac{1}{2}\rho v^2 (C_{B,d} - C_{B,c}) \\ 0 \end{pmatrix}, \tag{26}$$

where the perturbation has only effect in the along-track direction, since the absolute spacecraft velocity v is taken instead of the velocity relative to the atmosphere, and near-circular orbits are considered. Moreover the aforementioned value of the inter-satellite separation allows to neglect the differences in satellite absolute velocity and in the density at those positions (these assumptions would not be applicable for missions like GRACE or SWARM which present satellite separations of ≈ 200 km). Therefore the effect of the differential drag is produced due to the different ballistic coefficient of the deputy and chief satellites. The trend over time of the perturbation is dominated by the behavior of the atmospheric density.

A perturbation model as Equation (26) can be treated in a straightforward manner in the Cartesian frame: the overall effect impacts only the local tangential direction and the in-plane and out-of-plane equations of motions are decoupled.

The weak point of Equation (26) is represented by the lack of an analytical model able to realistically represent the main features of the atmospheric density properties (Kumar et al., 2011).

5.1 General empirical expression for the differential drag

The modeling of the effects produced by the differential aerodynamic drag on the relative motion, as discussed here in the following, is inspired by the results of

Colombo (1989). In his work Colombo addresses the dynamic aspects of the orbit determination errors analyzing how the system of equations of linearized dynamics of near-circular orbits (i.e., the HCW dynamical system) responds to acceleration errors. Colombo shows that the HCW system behaves like a filter with two sharp pass-bands centered on frequencies 0 and the orbital angular rate n. Therefore an empirical formulation of the acceleration errors comprising the sums of the Fourier components at that two resonant frequencies is able to represent the effects of the most general error function.

By applying these results to the relative motion problem, the following empirical model for the differential drag can be defined:

$$\mathbf{d}^{\mathrm{RTN}}_{\text{d-drag, emp}} = \begin{pmatrix} 0 \\ A\cos(nt) + B\sin(nt) + C \\ 0 \end{pmatrix}, \tag{27}$$

with the acceleration having a general harmonic expression in the along-track direction. A and B are the amplitudes of the once-per-orbit periodic part, whereas C is the mean value of the perturbation acceleration.

It is emphasized that this empirical approach can be employed for modeling other constant and once-per-orbit periodic acceleration contributions, depending on the focus of the application. For high area-to-mass ratio and small length-scale spacecraft formation flying applications, for example, the solar radiation pressure can be used as means of formation control (Mingotti and McInnes, 2013). Such control accelerations can be recast adopting the general empirical expression of Equation (27) on the three local directions, depending on the Sun-direction geometry.

In agreement with the approach sketched in Figure 5, the analytical expressions for the relative state $\mathbf{x}(t)$ forced by Equation (27) (provided in Colombo (1989)) are mapped into ROEs.

The obtained expression of the relative semi-major axis is given by:

$$a\delta a(t) = a\delta a_0 + \frac{2t}{n}C + \frac{2(1-\cos(nt))}{n^2}B + \frac{2}{n^2}\sin(nt)A. \tag{28}$$

It is emphasized that the simple expression of Equation (28) is also obtained when the perturbation assumes the general empirical form in all three components, since in-plane and out-of-plane components are decoupled and $a\delta a = 4x + 2\dot{y}/n$.

According to Equation (28), the mean value of the differential drag produces a linear variation of the relative semi-major axis in time. The periodic components, instead, produce some oscillations superposed to the mean behavior.

The expression of the relative mean longitude is given by:

$$a\delta\lambda(t) = a\delta\lambda_0 - \frac{3}{2}na\delta a_0 t - \frac{3}{2}t^2C - \frac{3(nt-\sin(nt))}{n^2}B - \frac{3(1-\cos(nt))}{n^2}A. \tag{29}$$

The mean value of the differential drag produces a quadratic term in time, whereas the periodic components provide constant, linear and periodic contributions.

The remaining in-plane ROE is the relative eccentricity vector which is affected by the empirical acceleration as follows:

$$\begin{aligned} a\delta e_x(t) &= a\delta e_{x0} + \frac{2\sin(nt)}{n^2}C + \frac{\sin^2(nt)}{n^2}B + \frac{nt+\cos(nt)\sin(nt)}{n^2}A, \\ a\delta e_y(t) &= a\delta e_{y0} + \frac{2(1-\cos(nt))}{n^2}C + \frac{nt-\cos(nt)\sin(nt)}{n^2}B + \frac{\sin^2(nt)}{n^2}A, \end{aligned} \tag{30}$$

where the only linear in time effects are generated by the amplitudes A and B respectively on the x and y components of the relative eccentricity vector.

Equations (28)-(30) constitute a ROE-based model that generalizes the results of different formulations available in the literature. In Leonard et al. (1989), a Cartesian approach is used and the differential drag is modeled by a constant acceleration (i.e., $A = B = 0$) thus achieving a model not able to capture the possible linear in time variation of the relative eccentricity vector. In Gaias et al. (2013) the constant differential drag is simply reproduced through a variation of the relative semi-major axis linearly in time. Subsequently, this effect determines a quadratic in time behavior of the relative mean longitude due to the relationship between δa and δu within the relative motion dynamics. Finally an approach based on the Gauss Variational Equations is employed in Ben-Yaacov and Gurfil (2013), using one-orbit averaged orbital elements and an exponential model for the atmospheric density. The paper shows that, for near-circular orbits, the difference in eccentricity is not controllable by means of the differential drag. This is in agreement with Equation (30), since the considered atmospheric density presents no periodical terms.

The interpretation of Equations (28)-(30) through ROEs suggests the introduction of three parameters to describe the mean time variations of some in-plane elements measured in m/s:

$$\begin{aligned} a\delta\dot{a} &= \tfrac{2}{n}C, \\ a\delta\dot{e}_x &= \tfrac{1}{n}A, \\ a\delta\dot{e}_y &= \tfrac{1}{n}B. \end{aligned} \tag{31}$$

Provided that their numerical values are known (e.g., through estimation, or numerical fitting from realistic simulations or flight data) they allow to build a simple state transition matrix for the relative motion parametrized in ROEs subject to differential aerodynamic drag:

$$\begin{pmatrix} a\delta\boldsymbol{\alpha} \\ a\delta\dot{a} \\ a\delta\dot{e}_x \\ a\delta\dot{e}_y \end{pmatrix}(t) = \begin{bmatrix} \boldsymbol{\Phi}_{\text{HCW}}(t,t_0) & \boldsymbol{\Phi}_{\text{d-drag}}(t,t_0) \\ \mathbf{O}_{3\times 6} & \mathbf{I}_{3\times 3} \end{bmatrix} \begin{pmatrix} a\delta\boldsymbol{\alpha}_0 \\ a\delta\dot{a}_0 \\ a\delta\dot{e}_{x0} \\ a\delta\dot{e}_{y0} \end{pmatrix}, \tag{32}$$

with:

$$\boldsymbol{\Phi}_{\text{d-drag}}(t,t_0) = \begin{bmatrix} dt & \frac{2}{n}\sin(u-u_0) & \frac{2}{n}(1-\cos(u-u_0)) \\ -\frac{3}{4}ndt^2 & -\frac{3}{n}(1-\cos(u-u_0)) & -3dt+\frac{3}{n}\sin(u-u_0) \\ \frac{\sin(u-u_0)}{n} & dt+\frac{\cos(u-u_0)\sin(u-u_0)}{n} & \frac{\sin^2(u-u_0)}{n} \\ \frac{1-\cos(u-u_0)}{n} & \frac{\sin^2(u-u_0)}{n} & dt-\frac{\cos(u-u_0)\sin(u-u_0)}{n} \\ 0 & 0 & 0 \\ 0 & 0 & 0 \end{bmatrix}. \tag{33}$$

This model is valid as long as the assumption of the parameters of Equation (31) being constant in time is acceptable.

5.2 Non-constant behavior of the differential drag perturbation

The variation over time of the differential drag perturbation is driven by the behavior of the atmospheric density. According to the assumed model (i.e., Equation (26)), the oscillation of the orbital velocity is negligible for near-circular orbits. Moreover the ballistic coefficients of the two satellite are constant for three-axis stabilized attitudes and no moving appendages. At a given orbit height, the density profile varies depending on the Sun-direction geometry, due to day and night transitions. Figure 7 shows the atmospheric density profile over two orbits time for a spacecraft on the chief orbit of Table 1 in two periods of the year and LTAN respectively of 12:00 and 09:30. The Jacchia 71 model is used to compute the density value; it can be noted that the density trend varies during the year (all plots share the same axis-scale).

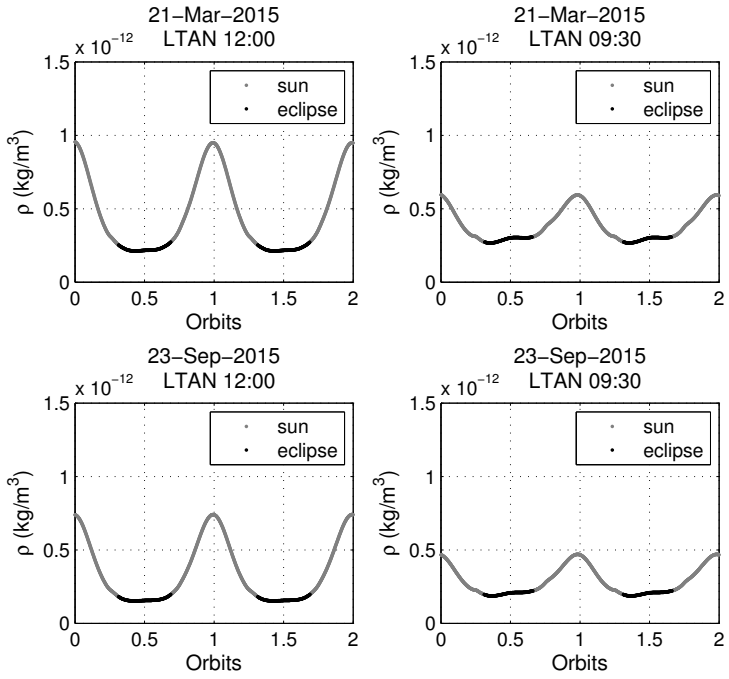

Fig. 7 Trend over time and seasonal effect of the atmospheric density (Jacchia 71 model) for the chief orbit of Table 1 at two different LTAN.

5.3 Numerical Validation

The numerical validation of the model is performed through the simulation setup previously described in Figure 5, where the atmospheric drag is the only perturbation taken into account. Therefore, the reference trajectories of the two satel-

lites are obtained via numerical integration subject to the absolute drag of Equation (25), with the density ρ computed through the Jacchia 71 model. The assumed spacecraft characteristics are customized on the satellites envisioned for the AVANTI experiment (Gaias et al., 2014): a roughly cubic shape 1 m side with a mass at launch of approximately 140 kg main satellite and a one-unit picosatellite. The corresponding difference in the area to mass ratio S/m amounts to circa 0.0066 m^2/kg. The modeled ROEs $a\delta\boldsymbol{\alpha}^{model}$ are obtained from the analytical model provided in Equations (32) and (33). Dealing with the assessment of the accuracy of the model, the values of the mean linear variations of the relative semi-major axis and of the relative eccentricity vector are here derived via numerical fitting of the related $a\delta\boldsymbol{\alpha}^{\mathrm{ref}}$ profiles. In real applications, instead, these values have to be estimated, for example through the approach described in Ardaens and Gaias (2014).

The simulation here reported is based on the RO1 initial conditions of Table 1, with a scenario occurring in middle October 2015, LTAN 09:30, and the following numerical values for the mean time derivatives of relative semi-major axis and relative eccentricity vector:

$$\begin{aligned} a\delta\dot{a}_0 &= -2.76 \cdot 10^{-4}\,\mathrm{m/s}, \\ a\delta\dot{e}_{x\,0} &= -5.95 \cdot 10^{-5}\,\mathrm{m/s}, \\ a\delta\dot{e}_{y\,0} &= +2.58 \cdot 10^{-5}\,\mathrm{m/s}. \end{aligned} \tag{34}$$

Figure 8 shows the in-plane ROEs over time: the reference elements $a\delta\boldsymbol{\alpha}^{\mathrm{ref}}$ are in gray whereas the modeled $a\delta\boldsymbol{\alpha}^{\mathrm{model}}$ are in black. Referring to the plots, the modeled ROEs faithfully track the reference ones, therefore the developed model is able to reproduce all meaningful aspects of the considered dynamics. For this simulation scenario, the effect of the atmospheric drag determines an average decrease of the relative semi-major axis of circa 23 meters over one day. The effect on the relative eccentricity vector is more pronounced on the x component where it amounts to circa 5 m of change over one day. Nevertheless, by referring to Figure 7, it can be noted that the oscillations of the density value occurring for the scenario October-LTAN 09:30 are less marked with respect to an orbit of LTAN 12:00 in the same period. In this latter case, the change of the x component of the relative eccentricity vector reaches the value of circa 12 m over one day.

According to Equation (30), the mean changes of the relative eccentricity vector have to be related to an oscillating behavior of the applied perturbation. Figure 9 presents the along-track components of the reference perturbation (plotted in gray) and of the approximating empirical function (plotted in black) employed to achieve the results of Figure 8. The two functions present almost the same mean values (i.e., upper view, solid gray and dashed black lines) thanks to the numerical fitting accomplished to determine $a\delta\dot{a}_0$, which is related to C through Equation (31). The maximum and minimum peaks, instead, do not match, since the employed empirical model retains only the terms at one-orbital-period frequency. The amplitude spectrum of both the along-track components is shown in the bottom view Figure 9: the reference acceleration presents also non-vanishing contributions at multiples of the orbital angular rate n. Therefore, the accuracy achieved by the model of Equations (32) and (33) represents a numerical evidence of the filtering action of the relative motion dynamical system.

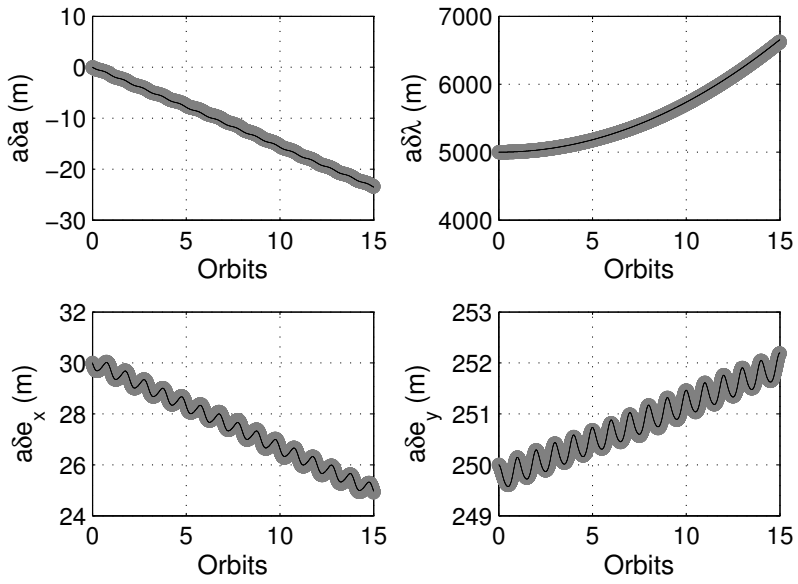

Fig. 8 Comparison of the in-plane ROEs over time: modeled $a\delta\boldsymbol{\alpha}^{model}$ (black-thin) and reference $a\delta\boldsymbol{\alpha}^{ref}$ (gray-thick), when differential drag is the only perturbation included.

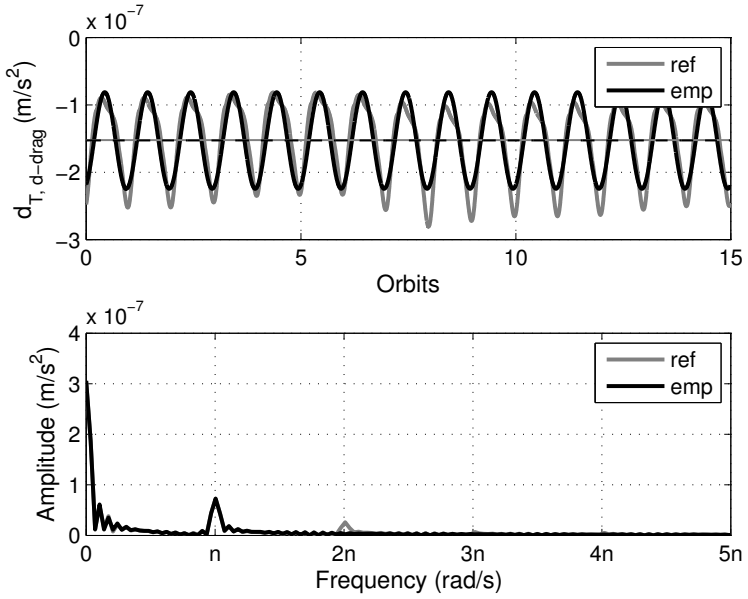

Fig. 9 Comparison of the along-track component of the differential drag acceleration: empirical (black) and reference (gray).

At a qualitative level, the effect produced by the harmonic profile of the differential drag can also be seen as a sequence of once-per-orbit "kicks" in the along-track direction, corresponding to the whole effect of the differential drag over one orbit. Recalling the geometrical interpretation of the effects of impulsive maneuvers on ROEs (Gaias and D'Amico, 2014), the mean argument of latitude at which these impulses take place is equal to the phase change of the relative eccentricity vector:

$$\phi = \arctan\left(\frac{a\delta\dot{e}_y}{a\delta\dot{e}_x}\right). \tag{35}$$

The equivalent delta-v of each single kick amounts to:

$$\delta v_T = \frac{n}{2}\Delta t\sqrt{a\delta\dot{e}_x^2 + a\delta\dot{e}_y^2}, \tag{36}$$

where Δt is the period of one orbit. Figure 10 reports the density profile over the mean argument of latitude. The vertical black line identifies the kicks location computed via Equation (35). The vertical gray lines, instead, mark the position of the mid point of the interval in which the spacecraft lay in eclipse.

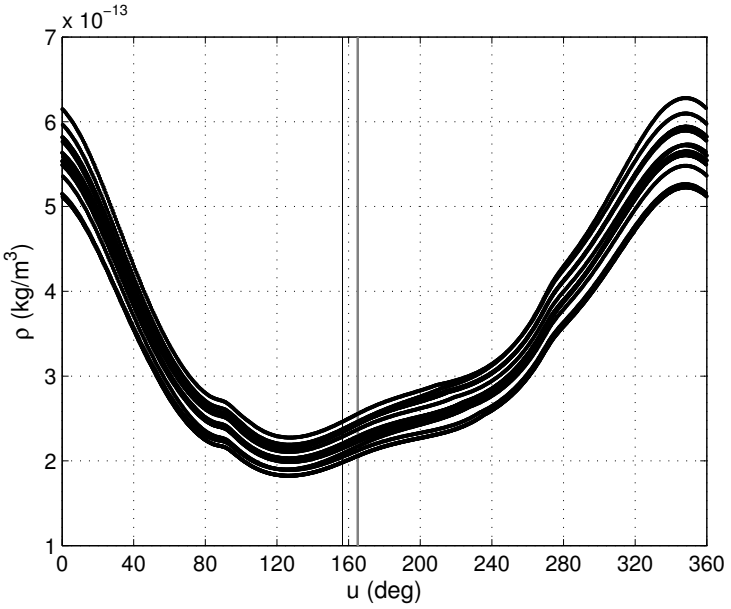

Fig. 10 Atmospheric density trend over the spacecraft mean argument of latitude.

6 The complete relative motion model

A comprehensive model for the relative motion between satellites in near-circular orbits can be assembled from the results developed in Sections 3 and 5, by exploiting the linearity of the problem. Despite its simplicity, this model represents

the most general case in low-Earth-orbits, since it accounts for all the dominant perturbations that occur in this environment (D'Amico, 2010, p. 32-33).

The relative state expressed in ROE is complemented with the three constant additional parameters defined in Equation (31) to generate the complete state ζ. Therefore, the complete state transition matrix is given by:

$$\begin{aligned} \boldsymbol{\zeta} &= \left(a\delta\boldsymbol{\alpha},\, a\delta\dot{a},\, a\delta\dot{e}_x,\, a\delta\dot{e}_y \right)^{\mathrm{T}}, \\ \boldsymbol{\zeta}(t) &= \begin{bmatrix} \boldsymbol{\Phi}_{\mathrm{HCW}}(t,t_0) + \boldsymbol{\Phi}_{\mathrm{J2}}(t,t_0) & \tilde{\boldsymbol{\Phi}}_{\text{d-drag}}(t,t_0) \\ \mathbf{O}_{3\times 6} & \mathbf{I}_{3\times 3} \end{bmatrix} \boldsymbol{\zeta}_0, \end{aligned} \tag{37}$$

with:

$$\tilde{\boldsymbol{\Phi}}_{\text{d-drag}}(t,t_0) = \boldsymbol{\Phi}_{\text{d-drag}}(t,t_0) + \begin{bmatrix} 0 & \mathbf{O}_{1\times 2} \\ -\frac{21}{8}\gamma H(\eta+1)ndt^2 & \mathbf{O}_{1\times 2} \\ \mathbf{O}_{3\times 1} & \mathbf{O}_{3\times 2} \\ +\frac{21}{8}\gamma \sin(2i)ndt^2 & \mathbf{O}_{1\times 2} \end{bmatrix}, \tag{38}$$

with respect to the previous expressions, the additional term of Equation (38) accounts for the joint effect of J_2 and differential drag. The relative semi-major axis varies linearly in time due to the differential drag (i.e., $a\delta\dot{a}_0$) and it determines an action on $\delta\lambda$ and δi_y due to the presence of the J_2 term. For near-circular (i.e., $\eta \approx 1$) low-Earth SSO (i.e., $H \approx -1$) orbits, the joint J_2-drag coefficient multiplying $a\delta\dot{a}_0$ is 7γ times smaller than the drag-only term. The component $(6,1)$ of $\tilde{\boldsymbol{\Phi}}_{\text{d-drag}}$ produces a small effect that couples the in-plane perturbation to the relative inclination vector.

6.1 Numerical validation

The numerical validation performed at the current level of development corresponds to the accuracy assessment of the whole model. To this end, a simulation setup which combines the features from the previously described dedicated environments is used. Inputs consist in the osculating Keplerian elements of the chief satellite at time t_0, the initial dimensional ROEs, and the numerical values of the additional parameters. The modeled state evolves through Equations (37) and (38). The modeling error is defined as the difference between the ROEs extracted from $\boldsymbol{\zeta}(t)^{\text{model}}$ and the reference values $a\delta\boldsymbol{\alpha}^{\text{ref}}$. These latter quantities are computed from the inertial states of the two satellites, which are numerically propagated. At this stage, the satellites are subject to a more general set of disturbances comprising: a 30 order and degree Earth gravitational potential, atmospheric aerodynamic drag, solar radiation pressure, Sun and Moon gravitational perturbation, tidal perturbation, and relativity effect.

The initial conditions considered correspond to RO1 and RO2 of Table 1 for a scenario occurring in October 2015, LTAN 9:30, and spacecraft characterized by a difference in area to mass ratio of 0.0066 m^2/kg.

For this validation purpose the numerical values of the initial additional parameters required by our analytical model are obtained through numerical fitting of the reference simulated data over the complete simulation horizon. Regarding

the results presented in Figures 11 and 12, they amount to:

$$\begin{aligned} a\delta\dot{a}_0 &= -2.97 \cdot 10^{-4}\,\mathrm{m/s}, \\ a\delta\dot{e}_{x\,0} &= -4.78 \cdot 10^{-5}\,\mathrm{m/s}, \\ a\delta\dot{e}_{y\,0} &= +4.98 \cdot 10^{-5}\,\mathrm{m/s}. \end{aligned} \tag{39}$$

Figure 11 presents the obtained modeling errors over time for RO1: each subplot focuses on a single component of the ROE vector. The error performed in $a\delta\lambda$ builds up as soon as the $a\delta a$ value deviates from the reference one. The remaining ROEs are modeled within the meter accuracy throughout the whole time horizon. Clearly accuracy results are determined by the accuracy in the knowledge (or in the estimation) of the additional parameters over the considered interval of time.

Figure 12 shows the modeling errors achieved assuming RO2 as initial conditions for the relative orbit. Since the chief orbit scenario is not changed, the numerical values of Equation (39) are still kept. The error achieved remains of the same order of accuracy gained before, despite that the mean relative longitude $a\delta\lambda$ at the final time amounts to circa 35 km, due to the joint action of the initial drift and of the differential drag. To conclude, the joint J_2-drag effects on the relative mean longitude and on the y component of the relative inclination vector, for this scenario and the $a\delta\dot{a}_0$ value of Equation (39), amount to circa 5.5 and 0.8 meters respectively over one day of propagation.

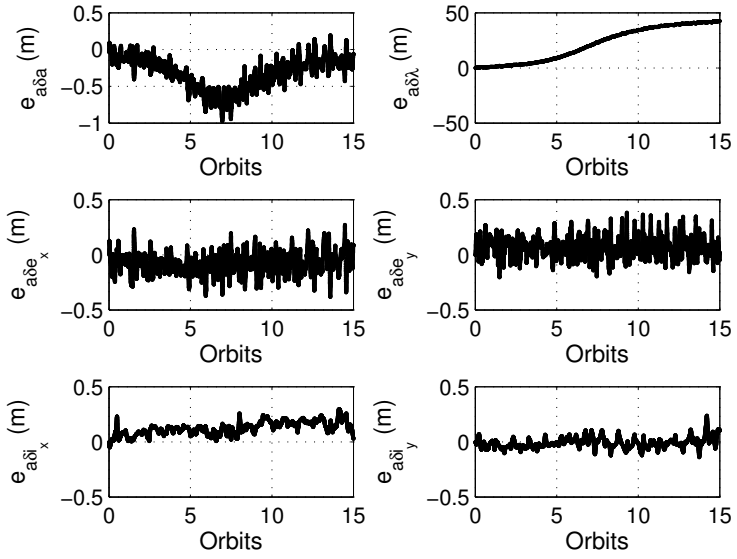

Fig. 11 Trend over time of the modeling errors in each ROE component for the simulation scenario RO1 of Table 1. Satellites are subject to a general set of perturbations.

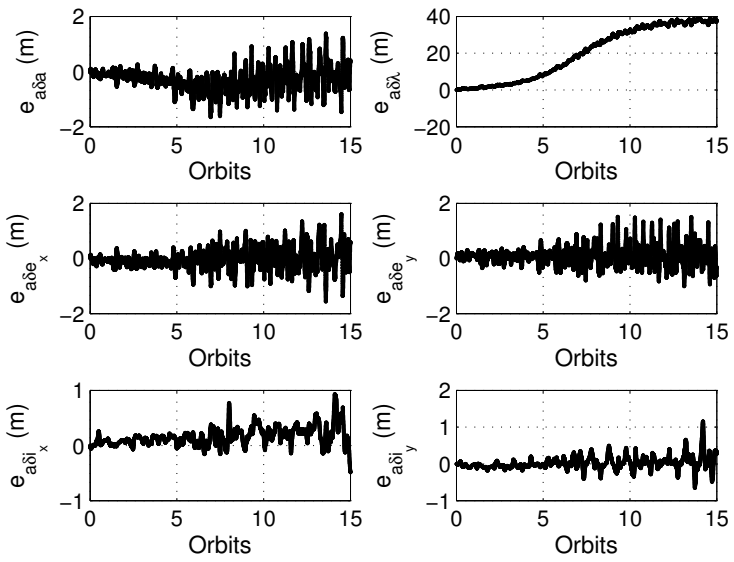

Fig. 12 Trend over time of the modeling errors in each ROE component for the simulation scenario RO2 of Table 1. Satellites are subject to a general set of perturbations.

7 Validation using flight data

This last section presents the validation of the improved model using flight data. The former relative motion model was able to reflect accurately the data from SAFE and TAFF, since both these experiments dealt with precise formation control of almost bounded relative orbits in mission scenarios where differential drag could be neglected. During the ARGON experiment performed in the course of the extended phase of the Prototype Research Instruments and Space Mission Technology Advancement (PRISMA) mission (Bodin et al., 2012), instead, a rendezvous of 30 km has been accomplished over less than one week, thus requiring a large relative semi-major axis to reduce the inter-satellite separation.

The data here considered were collected on the 25$^{\text{th}}$ of April 2012, from 02:00 to 16:00. At that time the relative semi-major axis achieved its largest value (i.e., -132 m), the relative orbit presented relative eccentricity and inclination vectors in anti-parallel configuration with magnitudes of 300 and 250 meters respectively, and, at the beginning of the data arc, the two satellites were separated of 23.5 km. During the considered time span no maneuvers have been performed.

Regarding the validation, the *reference* orbits come from the GPS-based precise orbit determination (POD) products (Ardaens et al., 2011b), which were delivered on daily basis during PRISMA and, in this case, exploited circa 20 hours of data from both GPS receivers. Consequently, reference ROEs are computed from the two satellite inertial states as depicted in Figure 2.

Figure 13 presents the trends of the $a\delta a$ and $a\delta i_x$ components (i.e., the elements that play a role in the J_2 modeling) of the reference ROE state. The linear fitting of

such reference data is plotted in black. Regarding $a\delta a$, the thin black line shows the fitting obtained when the differential drag effects are neglected (i.e., as performed during ARGON); whereas the thick black line includes a time derivative of the relative semi-major axis $a\delta\dot{a}_0$ of $-7.45 \cdot 10^{-6}$ m/s.

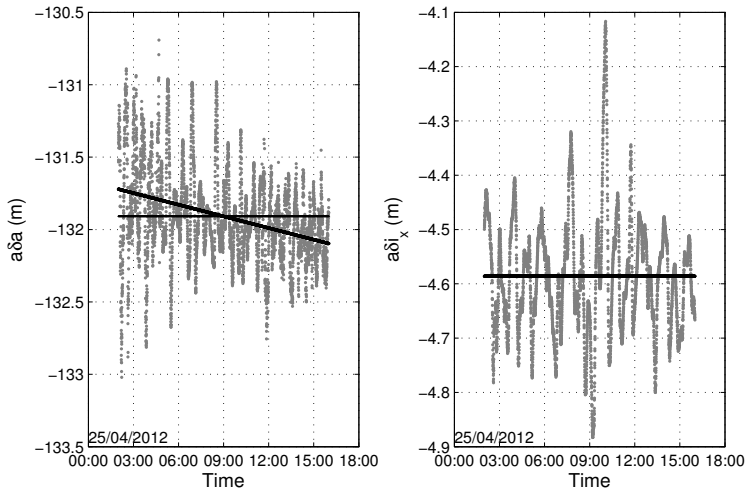

Fig. 13 Two components of the reference ROE state during ARGON: true elements (gray), their linear fitting (black).

In order to assess the modeling errors, the initial values of the fitted components are assumed as initial state (i.e., $a\delta\boldsymbol{\alpha}_0^{\mathrm{ref}}$). Figure 14 presents the differences between $a\delta\boldsymbol{\alpha}^{\mathrm{model}}$ and $a\delta\boldsymbol{\alpha}^{\mathrm{ref}}$ of the $a\delta\lambda$ and $a\delta i_y$ components for the former (in gray) and improved (in black) models. The error in the $a\delta\lambda$ component is due to the combined action of having neglected the differential drag effect and the non-vanishing relative semi-major axis. Even thought it is reasonable to neglect differential drag effects for satellites flying on a 750 km orbit (i.e., like accomplished in the PRISMA mission), the improvements offered by the revisited model become relevant when propagating the relative state over several hours.

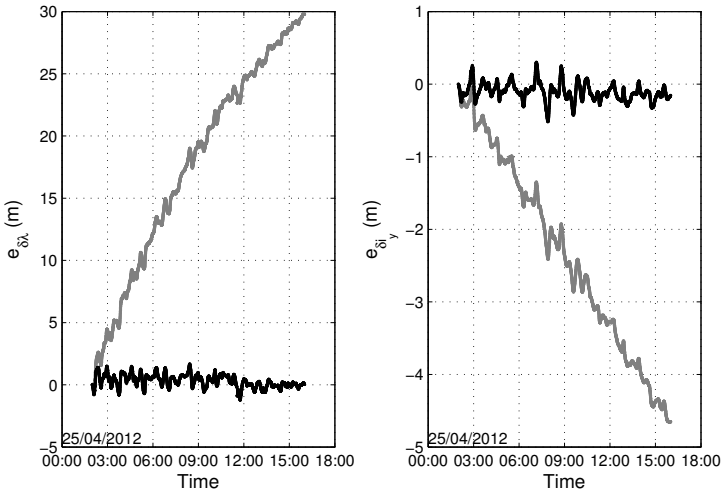

Fig. 14 Modeling error during ARGON: improved model (black), former model (gray).

8 Conclusions

This paper addresses the modeling of the relative motion between satellites flying in near-circular low-Earth-orbits. The proposed formulation evolves from the relative orbital elements based model extensively and successfully employed to support several recent in-flight formation flying activities. The result slightly improves the modeling of the Earth's oblateness J_2 perturbation. Moreover it complements the former version with the treatment of the differential aerodynamic drag perturbation.

By dealing with low-Earth-orbits, focus has been given to the aforementioned orbital disturbances. Nevertheless, the proposed approach is applicable to represent the effects produced by a general non-conservative perturbation, provided that the related additional parameters are estimated.

The proposed model is parametrized through relative orbital elements, therefore its validity is not restricted to close inter-satellite separations. The employed relative state provides an immediate geometrical understanding of the relative orbit. In addition, this formulation can benefit from the rich relative orbital elements framework, which also comprises the passive safety definition and a useful geometrical interpretation of the effects of impulsive maneuvers.

The relative motion model proposed in this paper has been developed to support the relative orbit determination and autonomous maneuver planning algorithms required by the incoming Autonomous Vision Approach Navigation and Target Identification experiment.

References

J.-S. Ardaens and S. D'Amico. Spaceborne Autonomous Relative Control System for Dual Satellite Formations. *Journal of Guidance, Control, and Dynamics*, 32 (6):1859–1870, 2009.

J.-S. Ardaens and G. Gaias. Spaceborne Autonomous Vision-Based Navigation System for AVANTI. Toronto, Canada, 2014. 65$^{\text{th}}$ International Astronautical Congress.

J.-S. Ardaens, S. D'Amico, and D. Fischer. Early Flight Results from the TanDEM-X Autonomous Formation Flying System. St-Hubert, Quebec, 2011a. 4$^{\text{th}}$ International Conference on Spacecraft Formation Flying Missions & Technologies (SFFMT).

J.-S. Ardaens, S. D'Amico, and O. Montenbruck. Final Commissioning of the PRISMA GPS Navigation System. Sao Jose dos Campos, Brazil, 2011b. 22$^{\text{st}}$ International Symposium on Spaceflight Dynamics.

J.-S. Ardaens, R. Kahle, and D. Schulze. In-Flight Performance Validation of the TanDEM-X Autonomous Formation Flying System. Munich, Germany, 2013. 5$^{\text{th}}$ International Conference on Spacecraft Formation Flying Missions & Technologies (SFFMT).

O. Ben-Yaacov and P. Gurfil. Long-Term Cluster Flight of Multiple Satellites Using Differential Drag. *Journal of Guidance, Control, and Dynamics*, 36(6):1731–1740, 2013. doi: 10.2514/1.61496.

R. Bevilacqua and M. Romano. Rendezvous Maneuvers of Multiple Spacecraft Using Differential Drag Under J2 Perturbation. *Journal of Guidance, Control and Dynamics*, 31(6):1595–1607, 2008.

P. Bodin, R. Noteborn, R. Larsson, T. Karlsson, S. D'Amico, J.-S. Ardaens, M. Delpech, and J. C. Berges. Prisma formation flying demonstrator: Overview and conclusions from the nominal mission. Number 12-072, Breckenridge, Colorado, USA, 2012. 35$^{\text{th}}$ Annual AAS Guidance and Control Conference.

D. Brower. Solution of the problem of artificial satellite theory without drag. *Astronomical Journal*, 64(1274):378–397, 1959. doi: 10.1086/107958.

W. H. Clohessy and R. S. Wiltshire. Terminal Guidance System for Satellite Rendezvous. *Journal of the Aerospace Sciences*, 27(9):653–658, 1960.

Oscar L. Colombo. The dynamics of global position system orbits and the determination of precise ephemerides. *Journal of Geophysical Research*, 94:9167–9182, 1989.

S. D'Amico. Relative Orbital Elements as Integration Constants of Hill's Equations. DLR-GSOC TN 05-08, Deutsches Zentrum für Luft- und Raumfahrt, Oberpfaffenhofen, Germany, December 2005.

S. D'Amico and O. Montenbruck. Proximity Operations of Formation Flying Spacecraft using an Eccentricity/Inclination Vector Separation. *Journal of Guidance, Control and Dynamics*, 29(3):554–563, 2006. doi: 10.2514/1.15114.

S. D'Amico, J.-S. Ardaens, and R. Larsson. Spaceborne Autonomous Formation-Flying Experiment on the PRISMA Mission. *Journal of Guidance, Control, and Dynamics*, 35(3):834–850, 2012. doi: 10.2514/1.55638.

S. D'Amico, J.-S. Ardaens, G. Gaias, H. Benninghoff, B. Schlepp, and J. L. Jørgensen. Noncooperative Rendezvous Using Angles-Only Optical Navigation: System Design and Flight Results. *Journal of Guidance, Control, and Dynamics*, 36(6):1576–1595, 2013. doi: 10.2514/1.59236.

Simone D'Amico. *Autonomous Formation Flying in Low Earth Orbit*. PhD thesis, Technical University of Delft, The Netherlands, March 2010.

J. R. Dormand and P. J. Prince. A family of embedded Runge-Kutta formulae. *Journal of Computational and Applied Mathematics*, 6(1):19–26, 1980.

G. Gaias, S. D'Amico, and J.-S. Ardaens. Generalized Multi-Impulsive Maneuvers for Optimum Spacecraft Rendezvous. Munich, Germany, 2013. 5$^{\text{th}}$ International Conference on Spacecraft Formation Flying Missions & Technologies (SFFMT).

G. Gaias, J.-S. Ardaens, and S. D'Amico. The Autonomous Vision Approach Navigation and Target Identification (AVANTI) Experiment: Objectives and Design. Porto, Portugal, 2014. 9$^{\text{th}}$ International ESA Conference on Guidance, Navigation & Control Systems.

Gabriella Gaias and Simone D'Amico. Impulsive Maneuvers for Formation Reconfiguration using Relative Orbital Elements. *Journal of Guidance, Control, and Dynamics*, 2014. accessed April 25 2014, doi: 10.2514/1.G000189.

A. Härting, C. K. Rajasingh, M. C. Eckstein, A. F. Leibold, and K. N. Srinivasamurthy. On the collision hazard of colocated geostationary satellites. Number 88-4239, Minneapolis, USA, 1988. AIAA/AAS Astrodynamics conference.

Y. Ichimura and A. Ichikawa. Optimal Impulsive Relative Orbit Transfer Along a Circular Orbit. *Journal of Guidance, Control and Dynamics*, 31(4):1014–1027, 2008. doi: 10.2514/1.32820.

B. S. Kumar, A. Ng, K. Yoshihara, and A. De Ruiter. Differential Drag as a Means of Spacecraft Formation Control. *IEEE Transactions on Aerospace and Electronic Systems*, 47(2):11251135, 2011.

M. Lara and P. Gurfil. Integrable approximation of j2-perturbed relative orbits. *Celestial Mechanics and Dynamical Astronomy*, 114(3):229–254, 2012. DOI: 10.1007/s10569-012-9437-8.

C. L. Leonard, W. M. Hollister, and E. V. Bergmann. Orbital Formationkeeping with Differential Drag. *Journal of Guidance, Control, and Dynamics*, 12(1):108–113, 1989. doi: 10.2514/3.20374.

T. A. Lovell and S. G. Tragesser. Guidance for relative motion of low earth orbit spacecraft based on relative orbit elements. Number 04-4988, Providence, Rhode Island, USA, 2004. AIAA Guidance, Navigation and Control Conference and Exhibit.

Vladimir Martinusi and Pini Gurfil. Solutions and periodicity of satellite relative motion under even zonal harmonics perturbations. *Celestial Mechanics and Dynamical Astronomy*, 111(4):387–414, 2011. doi: 10.1007/s10569-011-9376-9.

G. Mingotti and C. McInnes. High Area-to-Mass Ratio and Small Length-Scale Spacecraft Formation Flying Applications. Munich, Germany, 2013. 5$^{\text{th}}$ International Conference on Spacecraft Formation Flying Missions & Technologies (SFFMT).

O. Montenbruck, M. Kirschner, S. D'Amico, and S. Bettadpur. E/I-Vector Separation for Safe Switching of the GRACE Formation. *Aerospace Science and Technology*, 10(7):628–635, 2006. doi: 10.1016/j.ast.2006.04.001.

David Pérez and Riccardo Bevilacqua. Differential drag spacecraft rendezvous using an adaptive lyapunov control strategy. *Acta Astronautica*, 83:196207, 2013. http://dx.doi.org/10.1016/j.actaastro.2012.09.005.

David Pérez and Riccardo Bevilacqua. Lyapunov-Based Adaptive Feedback for Spacecraft Planar Relative Maneuvering via Differential Drag. *Journal of Guidance, Control, and Dynamics*, 37(5):1678–1684, 2014. doi: 10.2514/1.G000191.

David Pérez, Brendt Wohlberg, Thomas Alan Lovell, Michael Shoemaker, and Riccardo Bevilacqua. Orbit-centered atmospheric density prediction using artificial neural networks. *Acta Astronautica*, 98:9–23, 2014. doi: 10.1016/j.actaastro.2014.01.007.

H. Schaub and K. T. Alfriend. J2 invariant reference orbits for spacecraft formations. *Celestial Mechanics and Dynamical Astronomy*, 79(2):77–95, 2001.

Hanspeter Schaub and John L. Junkins. *Analytical Mechanics of Space Systems*. AIAA Ed. Series, 2003.

S. A. Schweighart and R. J. Sedwick. High-Fidelity Linearized J2 Model for Satellite Formation Flight. *Journal of Guidance, Control and Dynamics*, 25(6):1073–1080, 2002.

Andrew J. Sinclair, Ryan E. Sherrill, and T. Alan Lovell. Calibration of Linearized Solutions for Satellite Relative Motion. *Journal of Guidance, Control, and Dynamics*, 37(4):1362–1367, 2014. doi: 10.2514/1.G000037.

S. R. Vadali. Model for Linearized Satellite Relative Motion About a J2-Perturbed Mean Circular Orbit. *Journal of Guidance, Control and Dynamics*, 32(5):16871691, 2009. doi:10.2514/1.42955.

To the Editor and Reviewers of the paper **"Relative Motion Model with Time-Varying Differential Drag"**,

This document is intended to report the modifications further accomplished with respect to the first revision.
In the paper, all the applied changes are marked in blue.
Please be aware that we modified also the title of the paper (by following the suggestion of Reviewer 1).
Further details and considerations regarding your remarks are reported below.

Thanks again for the time you dedicated to our work.
Sincerely,
Gabriella Gaias

Answers to Reviewer 1:

1. Thanks for the suggestion. We do agree that it would be an improvement; therefore the title has been changed accordingly.

2. The expression "between two maneuvers" has been added in the last sentence of the second paragraph in page 2.

3. The former paragraph "For the AVANTI experiment … reflect coarsely the day-night variations of the density." has become independent and has been reformulated also in consideration of remarks by Reviewer 2.

4. Corrected citation style in the last paragraph in page.

5. Not addressed, following Editor's indication.

6. Punctuation added after each Equation appearing across the paper.

7. Full stop added to footnote of page 4.

8. Not addressed, following Editor's indication.

9. Paragraph under Equation (19), citation changed into: "Equation (2.28) developed in (D'Amico, 2010)".

10. Equations (21) and (23): corrected subscript notation for "J2".

11. Corrected expression "…the corresponding satellite's initial states …" in Section 3.1.

12. First paragraph of section 5.1, corrected verb "responds".

13. Figure 8.
    Among all the pictures that addressed the numerical validation of the ROE modelling, Figure 8 is the only one presenting the absolute ROE values instead of the errors between *true* and modeled quantities. This choice was accomplished in order to visualize at least once the effect of the differential-drag on the ROEs over time. Nevertheless, in this way the gray points are almost hidden by the black ones.
    In order to improve the readability of the plot, we changed the markers' type and size, and consequently, the caption.

14. Corrected transpose symbol in Equation (37).

15. Paragraph below Equation (38), "Φ6×1" changed into "The component (6,1) of Φ^{tilde}_{d-drag}… ", which assumes a non-vanishing value only in Equation (38).

16. Eighth line of the first paragraph of section 6.1, inserted correct expression "These latter quantities".

17. Section 6.1, second paragraph, corrected typo in "area to mass ratio".

18. Second paragraph of Section 7, verb "were" corrected. Added "~" in *tex* file to force "km" to remain attached to the number.

19. Yes, we realized that PRISMA appears for the first time only in Section 7, since earlier solely some of its specific experiments have been mentioned and referenced (e.g., SAFE and ARGON). Therefore, to acknowledge the mission and to introduce the PRISMA acronym, the first paragraph of Section 7 has been changed (and related reference has been added).

Answers to Reviewer 2

1. *In the response letter: "Concerning the AVANTI SW, we cannot even implement a simple model like Jacchia 71. And, as mentioned in the introduction, a precise model for the atmospheric density does not imply to be able to model precisely the differential drag force.* ***Anyway, this is not our objective. For us it is enough to capture the ROE trends****"?*
   Why can't/couldn't a simple model be implemented? Too heavy computationally?

The AVANTI flight software is a complete and complex GNC system that performs (at every call) different actions: retrieving images from the star-tracker, processing images to identify the target satellite, performing the relative orbit determination, computing/updating the required maneuvers' plan, and accomplishing the relative motion prediction used by the collision avoidance safety monitoring application (which, moreover, runs on a different thread with respect to the other listed AVANTI activities). At least the last three units require a relative motion model. Therefore, in order to fit into the real-time constraints, and to reduce the complexity of the software architecture, we could not opt for implementing a density model (even simple as Jacchia 71) together with the required integrator of the relative dynamics equations. We opted instead for the exploitation of semi-analytical methodologies to the largest possible extent, also in continuation with the design philosophy employed for SAFE (PRISMA mission) and TAFF (TanDEM-X). More information can be retrieved in the AVANTI related publications cited in the paper.

I agree that density is not the only parameter, but it is a "must-know" parameter for accurate DD modeling.

Sure that density modelling is a "must-know" for accurate DD modelling.

Nevertheless the point is that we are not aiming at modelling the DD but rather at having an understanding of its mean effects on the relative orbital elements (see first response letter: "**The second main contribution of the work consists in a general empirical formulation (very simple) to include the mean effects produced by non-conservative perturbations (like differential drag).**").

If our objective were to validate in-flight an accurate model of DD, instead, the space segment of the mission should be designed in a different way (e.g., sensors' set) with respect to the one hosting AVANTI. In particular, each spacecraft should be equipped with a GPS receiver to provide the navigation accuracies required for precise validation. AVANTI, on the contrary, aims at demonstrating pure vision-based approach (no relative GPS) to a noncooperative client satellite (no inter-satellite link).

2. *In the introduction: "Furthermore, the modeling of the differential drag is also greatly affected by the uncertainties regarding the knowledge of the attitude-dependent cross-sectional area and drag coefficient of the target spacecraft. As a result, a computationally-expensive precise model of the atmosphere density is not really mandatory. In fact, it is enough to focus on the global effect produced by the differential drag on the relative state using a low-accuracy model of the atmospheric density, provided that this model is able to reflect coarsely the day-night variations of the density."*

   Unless an explanation is provided, I cannot see the connection between saying that DD is affected by attitude and other parameters and saying that as a consequence we don't need an accurate density model.

   By considering this objection, we recognize that the paragraph in question has to be improved, in the attempt to explain better the motivation to opt for our proposed approach. Therefore the paper now presents a reformulated version.

Just as background information, here there follow some further explanations about such connection.

"**Furthermore, the… spacecraft.**"→ If one aims at precisely modelling the differential drag acceleration, one should have knowledge of and authority on the magnitude of all the error sources that are involved in the model.

"**As a result, … mandatory.**"→ In our case we have no knowledge and no control of all the DD-meaningful quantities of the target spacecraft. It, in fact, is a 1-unit cube-sat, with coarse attitude control capability and not capable to provide any reliable navigation information during the duration of the AVANTI experiment (navigation information which anyway could not be transmitted to the other spacecraft of the formation since no inter-satellite link is available). In this framework, there is no point to try to reduce the error committed in modeling the density if all the other sources of error could nullify such benefit.

"**In fact, it is enough … of the density.**"→In order to meet the AVANTI objectives, in fact, it is enough to estimate the global effects that the DD produces on the relative motion, within the accuracy realizable/meaningful during AVANTI (i.e., meter level). To this aim, a simple empirical formulation of the functional expression of Equation (27) can do the job thanks to: 1) the particular choice of the parameterization we adopted, 2) the filtering behavior of the linearized equations of motion that naturally filters out harmonic contributions of frequencies higher than one-orbital-period frequency.

The verification is provided in Figure (9), which clearly shows that the empirical acceleration differs from the *true* acceleration (we are not modelling the DD!). Nevertheless, it is capable to reflect the effect of the *true* DD acceleration, since the modeled relative orbital elements ROEs remain within an acceptable (for AVANTI) accuracy with respect to the *true* ones (Figure 8).

What about solar storms? Those cause variations that are way outside of a regular day-night variation.

Given the sensors' set and consequent accuracies in play during AVANTI, for all the considerations already mentioned, we would not be able anyway to distinguish which phenomenon produced a certain specific effect.

This is exactly the benefit of our approach. We do not bother of modeling phenomena that anyway we are not able to precisely manage. But we try to include their effect; provided that they influence the mean evolution of the relative orbital elements (thus such effect would be absorbed by the numerical values of the estimated parameters aDaDot, aDexDot, and aDeyDot of Equation (31)).

Why it is enough to focus on the global effect? This sounds like a bold statements, not supported by numbers.

This is not a bold statement but rather one of the main contributions of the paper addressed in many parts of the work, namely: second and third items in page3, Section 5.1, Section 5.3, and Section 7. Not only has it been supported by numerical validation, but also by the post-analysis of the flight data collected during ARGON. In Section 7, in fact, it was shown that a benefit of estimating aDaDot would have occurred also for the relative navigation accomplished during ARGON (see Figure 13). Given the height of the PRISMA mission orbit and the fact that during the

experiment (i.e., in April) it was not subject to eclipses, there was no need/benefit in estimating also aDexDot, and aDeyDot.

This paper mentions differential drag in the title, thus, more accuracy is expected in dealing with it, and the above statements need deeper explanations, and in the second case a backup (citation, simulations, etc.).

Two among the works cited within the paper (i.e., Leonard et al. (1989) and Bevilacqua and Romano (2008)) also present the wording "Differential Drag" in the title, despite 1) differential drag is modeled as piece-wise constant with further assumptions on how the control authority is realized; 2) a Cartesian parameterization is used, which is valid only for inter-satellite separations of the order of one kilometer (close-formations); 3) from an operational point of view, the control of a close-formation would hardly be accomplished by means of a DD-based approach, due to the difficulties in realizing a fine control and collision avoidance considerations.

Nevertheless both papers offer research-relevant insights not one-to-one related to how precisely the differential drag acceleration is modelled.

Probably this objection is driven by the misunderstanding concerning the precise modeling of the differential drag perturbation. We are not claiming to be able to perform any precise modelling of the differential drag acceleration but rather to exploit an empirical formulation that reflects (to an operational meaningful accuracy) its effects on the relative motion in near-circular low-Earth-orbits.